A near-infrared large Stokes shift probe based enhanced ICT strategy for F- detection in real samples and cell imaging

Qinghua Hu, Qiuxiang Huang, Yu Mao, Xinlin Liu, Fangrong Tan, Yuyuan Wang, Qiang Yin, Xumeng Wu, Hongqing Wang

PII: S0040-4020(19)31155-X

DOI: https://doi.org/10.1016/j.tet.2019.130762

Reference: TET 130762

To appear in: *Tetrahedron*

Received Date: 15 September 2019

Revised Date: 29 October 2019

Accepted Date: 1 November 2019

Please cite this article as: Hu Q, Huang Q, Mao Y, Liu X, Tan F, Wang Y, Yin Q, Wu X, Wang H, A near-infrared large Stokes shift probe based enhanced ICT strategy for F- detection in real samples and cell imaging, *Tetrahedron* (2019), doi: https://doi.org/10.1016/j.tet.2019.130762.

A near-infrared large Stokes shift probe based enhanced ICT strategy for F- detection in real samples and cell imaging

Qinghua Hu, Qiuxiang Huang, Yu Mao, Xinlin Liu, Fangrong Tan, Yuyuan Wang, Qiang Yin, Xumeng Wu, Hongqing Wang*

School of Chemistry and Chemical Engineering, Hunan key laboratory for the design and application of actinide complexes, University of South China, 28 Changsheng West Road, Hengyang, Hunan, 421001, PR China;

** Corresponding author: E-mail address: hqwang2015@126.com*

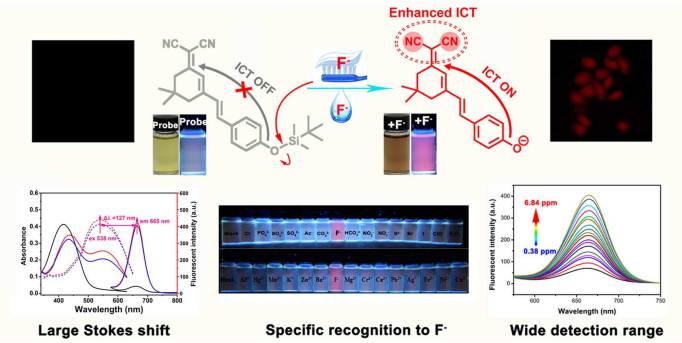

Abstract:

In view of the few reports of the near-infrared emissive probe for fluorine ions, we herein designed and synthesized a new easy-to-get colorimetric and near-infrared emissive fluorescent probe (**IS-NR-F**) with a large Stokes shift (>127 nm). Based on specific F^- triggered desilylation reaction induced enhanced ICT strategy involving the donor phenolate anion and the acceptor malononitrile, the probe exhibited dual colorimetric and fluorescent turn-on responses, and provided excellent selectivity for fluoride ions. The fluorescent response at 665 nm displayed very good linear relationship in the wide concentration range and deduced a low detection limit of 0.09 ppm. The detection mechanism was confirmed by ^1H NMR, ESI-MS, and TLC calculation. Moreover, probe **IS-NR-F** has been successfully employed to detect F^- in tap water, toothpaste samples, and fluorescent imaging of F^- in HeLa cells.

Keywords: Fluoride; Near-infrared fluorescence; Large Stokes shift; Fluorescent image

1. Introduction

The smallest and most negative anionic, fluorine ion (F^-), has been received great attention as an important chemical component in organisms and medical systems [1, 2]. Fluoride can be usually contacted through food, air, toothpaste, tea and medicines[3]. The intake of trace amount fluoride can not only prevent dental caries but help bone growth [4-6]. However, the World Health Organization (WHO) recommends fluoride levels should be less than 1.5 ppm in drinking water [7], and excessive ingestion of fluoride is likely to cause chronic poisoning, including dental fluorosis, bone fluorosis, metabolic dysfunction and urolithiasis [8, 9]. Therefore, given these widespread applications of F^- in daily life and its special function in a biological system, it has drawn greater attention to developing highly efficient and reliable methods for the detection and monitoring of F^- in drinking water as well as in the biological system.

The traditional methods including ion-selective electrodes [10], ion chromatography [11] and colorimetry [12] have been used for detecting fluorine ions. However, most of them couldn't be applied to detect F^- in a biological system. Compared to these traditional methods, the fluorescent probe technique could achieve easy, rapid and imaging in living cells and in vivo [13-34]. Especially, the near-infrared (NIR, 650-900nm) emissive fluorescent probe shows an excellent imaging performance in this aspect because of that its long-wavelength photons often perform a lower environmentally-induced light scattering, less interference from endogenous chromophores, and less photodamage [35-40]. In recent years, several

NIR fluorescent probes have been developed for F^- detection. However, most of them have small Stokes shifts(<35 nm) [41, 42], which may limit their further application in biosamples and decrease the detection sensitivity of probe to some degree because of the interference from excitation source with the "self-absorption" effect [43]. Thus, it remains attractive to develop NIR fluorophores from common raw materials with large Stokes shifts.

On the other hand, at present, most of the reported fluorescence probes have widely applied the two main strategies to detect F^- (**Table S1** and **Fig. S1**): a) hydrogen bonding interaction between F^- and OH group/NH group; b) Lewis acid\base interaction [44-55]. However, since F^- is the most electronegative anion and has strong hydration, the hydrogen bonding strategy would make the detecting process be largely hampered in protic solvent and could only be detected in a pure solvent or high content organic solvent that is harmful to cells [56]. For probes based on Lewis acid/base interaction, they could monitor fluoride in drinking water, and this strategy mainly includes fluorine-boron complexation [57-60] and desilylation reaction [61, 62]. Nevertheless, the fluorine-boron complexation is unstable and high cell toxicity [63] while the fluoride-triggered desilylation reaction relative to fluorine-boron complexation has had wide application in cell imaging and provides a specific irreversible recognition site due to the strong affinity between fluorine ion and silicon, thereby performing an excellent selectivity [64-67]. However, some of the probes based on desilylation reaction are still subject to the restriction for their short wavelength (UV-Vis light range) emission peak because they would suffer the

interference from endogenous chromophores and relative large photodamage to the biological system compared to NIR fluorescent probes [68-70].

Therefore, in order to solve the problem produced by the short-wavelength emission peak and achieve NIR fluorescent imaging in the cell, we proposed a novel NIR emissive fluorescence probe (**IS-NR-F,** Scheme 1B) by incorporating with a hydroxyl-functionalized dicyanoisophorone derivative and a tert-butyldimethylsilyl (TBDMS) group as the trigger moiety. To test the influence of the malononitrile group in **IS-NR-F** on the recognition of F^-, a control probe **IS-F (**Scheme 1A**)** lack of malononitrile group was also synthesized and tested in parallel with **IS-NR-F** for their sensing ability to F^-. Fortunately, as shown in Scheme 1, this strategy not only achieved the satisfactory NIR fluorescence around 665 nm with a remarkable Stokes shift (≥127 nm) in the existence of F^-, and **IS-NR-F** was used to monitor F^- in living cells successfully. Moreover, the probe displayed a low detection limit of 0.09 ppm and could be used for colorimetric detection of F^- in actual water samples and kinds of toothpaste with an excellent selectivity even in the presence of various cations and anions.

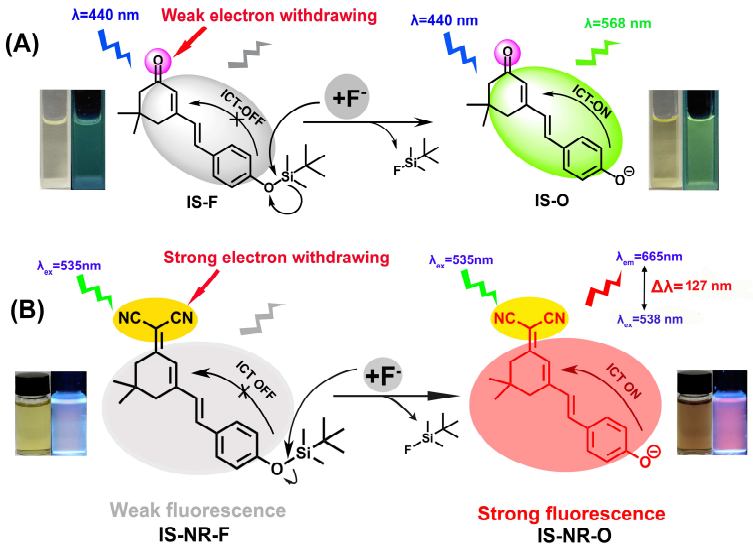

Scheme 1 The proposed sensing mechanism of probe **IS-F(A)** and **IS-NR-F (B)** for F^- recognition

2. Experimental

2.1. Material and methods

All chemicals (solvents, reagents and metal salts) were analytical grade, purchased from Aladdin (Shanghai, China) and used without further purification. The probe **IS-F** and **IS-NR-F** were dissolved in analytical grade DMSO for a stock solution (1 mM). The solution of anions (F^-, Cl^-, PO_4^{3-}, SO_3^{2-}, SO_4^{2-}, Ac^-, CO_3^{2-}, HCO_3^-, NO_2^-, NO_3^-, S^{2-}, Br^-, I^-, ClO^-) and cations (Al^{3+}, Hg^{2+}, Mn^{2+}, K^+, Zn^{2+}, Ba^{2+}, Mg^{2+}, Cr^{3+}, Ca^{2+}, Pb^{2+}, Ag^+, Fe^{3+}, Ni^{2+}, Cu^{2+}) were prepared by dissolving their sodium salt and nitrates in deionized water, respectively.

The UV-vis spectra were recorded through a Hitachi U-3900 spectrophotometer (made in Tokyo, Japan). Fluorescent spectra were measured in a Hitachi F-7000 spectrophotometer (made in Tokyo, Japan) in a 1 cm quartz cell. The ^1H NMR spectra were acquired on a Bruker 400 MHz spectrophotometer (made in Bruker, Germany) in deuterated dimethyl sulfoxide (DMSO-d_6) with tetramethylsilane as an internal

standard. The HR-MS was obtained on Alliance e2695-ACQUITY QDa (made in Waters, America) and LCMS-IT-TOF instrument (made in Shimadzu, Japan). The pH was performed on a model pHs-3C digital pH/mV meter (made in Shanghai, China). The cell fluorescent images were performed by a TE2000 inverted fluorescent microscope (made in Nikon, Japan).

2.2. Synthesis and characterization

The detailed synthetic procedure of probe **IS-F** and **IS-NR-F** were outlined in **Scheme 2**.

Synthesis of **IS-OH**: To a mixture solution of **a** (Isophorone) (1.38 g, 10 mmol) and p-hydroxybenzaldehyde (1.22 g, 10 mmol) in absolute EtOH (20 mL) was added EtONa (2.57 g, 15 mmol). The mixture was refluxed for 3 h, then 5 mL water was added to quench the reaction. The solvent was removed by vacuum rotary evaporation. Finally, the crude product was purified by silica gel (petroleum ether/ethyl acetate = 6:1, v/v) to give **IS-OH** as an orange solid (1.08 g, 44.6 % yield). ^{1}H NMR (400 MHz, DMSO-d_6, Fig. S2) δ (ppm) 9.81 (s, 1H), 7.50-7.48 (d, J = 8.0 Hz, 2H), 7.12-7.08 (d, J = 16.0 Hz, 1H), 6.97-6.93 (d, J = 16.0 Hz, 1H), 6.82-6.80 (d, J = 8.0 Hz, 2H), 6.01 (s, 1H), 2.53 (s, 2H), 2.24 (s, 2H), 1.06 (s, 6H). ^{13}C NMR (400 MHz, DMSO-d_6, Fig. S3): δ 199.28, 159.02, 156.11, 135.71, 129.51, 127.61, 126.62, 125.51, 116.19, 51.40, 38.61, 33.44, 28.48. HR-MS (Fig. S4): m/z (%): Calculated for $C_{16}H_{18}O_2$, 242.1307, found 265.1190 $[M+Na]^+$.

Synthesis of **IS-F:** To a solution of **IS-OH** (121 mg, 0.5 mmol) in dichloromethane (12 mL) and Et_3N (138 μL, 1 mmol), tert-butyldimethylsilyl chloride

(150.7 mg, 1 mmol) dissolved with 4 mL dichloromethane was added dropwise at 0 ºC. The mixture was stirred at room temperature for 12 hours. Then, the solvent was removed under reduced pressure. The resulting residue was purified by silica gel flash chromatography (eluted with petroleum ether/dichloromethane = 3:1, v/v) to afford the desired product as a yellow solid (106 mg, 59.6 % yield). ^{1}H NMR (400 MHz, DMSO-d_6, Fig. S5) δ (ppm): 7.57-7.55 (d, J = 8.0 Hz, 2H), 7.16-7.12 (d, J = 16.0 Hz, 1H), 7.04-7.00 (d, J = 16.0 Hz, 1H), 6.90-6.88 (d, J = 8.0 Hz, 2H), 6.04 (s, 1H), 2.52 (s, 2H), 2.25 (s, 2H), 1.06 (s, 6H), 0.98 (s, 9H), 0.23 (s, 6H). ^{13}C NMR (400 MHz, $CDCl_3$, Fig. S6): δ 200.23, 156.84, 155.20, 134.77, 129.35, 128.65, 127.57, 126.32, 120.25, 51.42, 39.10, 33.34, 28.51, 25.64, -4.39. HR-MS (Fig. S7): m/z (%): Calculated for $C_{22}H_{32}O_2Si$, 356.2172, found 379.2056 $[M+Na]^+$.

Synthesis of compound **b**: **an** (Isophorone) (3.455 g, 25 mmol) and malononitrile (1.980 g, 30 mmol) were dissolved in absolute EtOH (50 mL), followed by addition of piperidine (0.25 mL, 2.5 mmol) and glacial acetic acid (0.15 g, 2.5 mmol). Then, after the mixture was refluxed for 6 h under N_2 atmosphere, it was quenched with water, extracted with dichloromethane, dried over anhydrous sodium sulfate, filtered and concentrated in vacuo. Finally, the crude residue was purified by silica column chromatography (eluted with petroleum ether/dichloromethane = 1:3, v/v) to give **b** as a light yellow solid (3.63 g, 78 % yield). Melting point: 70.2-72.6 ºC. ^{1}H NMR (400 MHz, DMSO-d_6, Fig. S8) δ (ppm) 6.56 (s, 1H), 2.54 (s, 2H), 2.23 (s, 2H), 2.05 (s, 3H), 0.96 (s, 6H). ^{13}C NMR (400 MHz, DMSO-d_6, Fig. S9): δ 171.91, 162.98, 119.88, 113.93, 113.14, 76.50, 45.27, 42.42, 32.44, 27.75, 25.45. HR-MS (Fig. S10): m/z (%):

Calculated for $C_{12}H_{14}N_2$, 186.1157, found 185.1086 $[M-H]^-$.

Synthesis of **IS-NR-OH**: 20 mL acetonitrile was added to dissolve compound **b** (259 mg, 1.4 mmol) and p-hydroxybenzaldehyde (170 mg, 1.4 mmol), followed by five drops of piperidine. The mixture was refluxed for 5h under N_2 atmosphere and subsequently, the solvent was evaporated and removed through reduced pressure. The resulting residue was dissolved in 20 mL dichloromethane, washed with water (3×20 mL), and dried by anhydrous Na_2SO_4. After the removal of the solvent, the crude product was purified by column chromatography on silica gel (petroleum ether/dichloromethane=1:1, v/v) to afford the desired product as an orange solid (335 mg, 85.2% yield). Melting point: 200.4-201.5 ^oC. ^1H NMR (400 MHz, DMSO-d_6, Fig. S11) δ (ppm) 9.99 (s, 1H), 7.57-7.55 (d, J = 8.0 Hz, 2H), 7.22-7.23 (d, J = 4.0 Hz, 2H), 6.81-6.79 (m, 3H), 2.60 (s, 2H), 2.53 (s, 2H), 1.02 (s, 6H). ^{13}C NMR (400 MHz, DMSO-d_6, Fig. S12): δ 170.72, 159.81, 157.15, 138.74, 130.33, 127.59, 126.71, 121.84, 116.35, 114.58, 113.77, 75.28, 42.79, 38.67, 32.12, 27.91. ESI-HRMS (Fig. S13): m/z (%): Calculated for $C_{19}H_{18}N_2O$, 290.1419, found 313.1307 $[M+Na]^+$.

Synthesis of **IS-NR-F:** To a solution of **IS-NR-OH** (145 mg, 0.5 mmol) in dichloromethane (10 mL) and Et_3N (138 μL, 1 mmol), tert-butyldimethylsilyl chloride (150.7 mg, 1 mmol) dissolved with 5 mL dichloromethane was added dropwise at 0 ^oC. The mixture was stirred at room temperature for 12 hours. Then, the solvent was removed under reduced pressure. The resulting residue was purified by silica gel flash chromatography (eluted with petroleum ether/dichloromethane = 2:1, v/v) to afford the desired product as a yellow solid (158 mg, 78.2 % yield). ^1H NMR (400 MHz,

DMSO-d_6, Fig. S14) δ (ppm): 7.63-7.61 (d, J = 8.0 Hz, 2H), 7.26 (s, 2H), 6.89-6.87 (d, J = 8.0 Hz, 2H), 6.84 (s, 1H), 2.60 (s, 2H), 2.53 (s, 3H), 1.01 (s, 6H), 0.95 (s, 9H), 0.20 (s, 6H). ^{13}C NMR (400 MHz, DMSO-d_6, Fig. S15): δ 170.74, 157.13, 156.73, 137.94, 130.10, 128.13, 122.45, 120.81, 114.43, 113.62, 76.02, 42.78, 38.66, 32.01, 27.89, 25.96, 18.43, -4.07. ESI-HRMS (Fig. S16): m/z (%): Calculated for $C_{25}H_{32}N_2OSi$, 404.2284, found 427. 2175 $[M+Na]^+$.

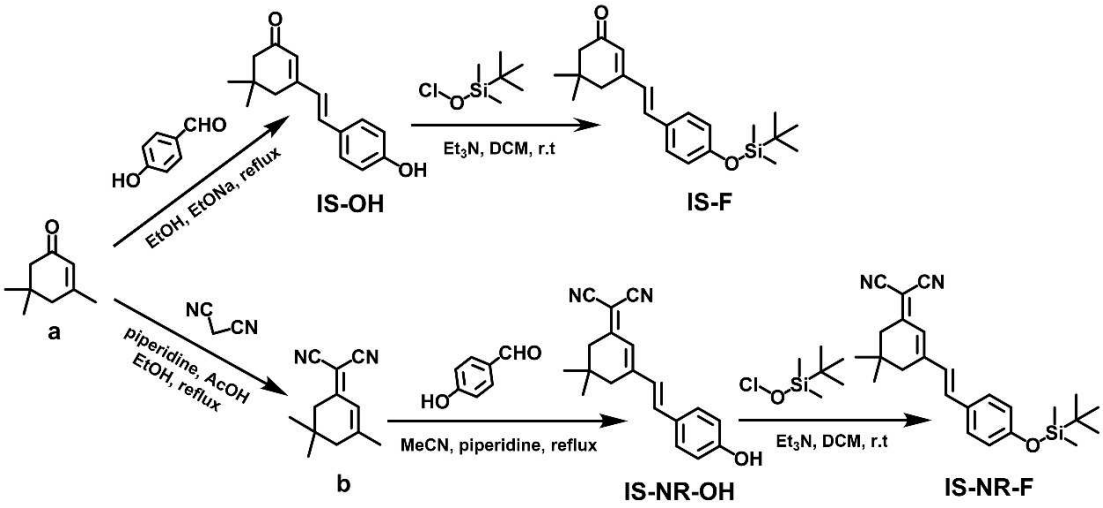

Scheme 2 The synthetic route of **IS-F** and **IS-NR-F**

2.3. UV-vis and fluorescent measurement

The **IS-F** and **IS-NR-F** were dissolved in DMSO as a stock solution (1.0 mM) while fluorine ion and other analytes were prepared by dissolving their sodium salt and nitrates in deionized water, respectively. All fluorescent and UV-vis spectral measurements were investigated in DMSO/PBS=1:1 (v/v, 20 mM, pH=7.4) solution at 37 ºC. The excitation and emission wavelength of fluorescent measurement for each fluorophore (for IS-F: λ_{ex} = 440 nm, λ_{em} = 568 nm and for IS-NR-F: λ_{ex} = 550 nm, λ_{em} = 665 nm) were measured respectively while their slit widths were 10.0 nm and 10.0 nm separately. Under the voltage of 450V or 550 V.

2.4. F^- detection in aqueous sample and kinds of toothpaste

One of the aqueous samples was collected directly from the tap water in our laboratory, and the other one that was filtered by membrane before used was collected from Xiangjiang River in Hengyang city. Then the pH value of the obtained solution was adjusted to 7.4 with NaH_2PO_4-Na_2HPO_4. Besides the F^- detection in aqueous water, the amount of F^- in commercially available toothpaste was also detected. To achieve the analysis of F^- in toothpaste, 1.0 g toothpaste was accurately weighed and dissolved in 10 mL PBS buffer solution (20 mM, pH=7.4) and stirred at 70 ºC. After 3 h, the fluorine-containing solution was obtained by filtering and 40 mL PBS buffer solution was added to the solution for further use.

2.5. Cell imaging and MTT assays

The toxicology of probe toward HeLa cells was determined by common methylthiazolyldiphenyl-tetrazolium bromide (MTT) assays. A certain density of HeLa cells was inoculated into 96-well plates and cultured at 37 ºC for 24 hours. Different concentrations of the probe were then added to the cells for staining and incubation continued for a further 24 hours. Finally, The HeLa cells were treated with 1 mg/mL of MTT (20 μL/well) in an incubator for 2 hours. After completion, the liquid in the well was carefully aspirated with a pipette, and the obtained crystal was dissolved in 150 μL DMSO, and the absorbance was recorded. Subsequently, the fluorescent imaging of HeLa cells was obtained. The HeLa cells were incubated with **IS-NR-F** for 1 hour at 37 ºC after washed with PBS buffer for two times. And then F^- was added into the cells for another 1 hour where the excessive **IS-NR-F** has been

removed with sterile PBS buffer first. The fluorescence images were collected with a TE2000 inverted fluorescent microscope (made in Nikon, Japan).

3. Results and discussion

3.1. Synthesis and characterization

The synthetic procedure of the probe **IS-F** and **IS-NR-F** were outlined in **Scheme 2**. Firstly, the isophorone based fluorophore **IS-OH** was readily synthesized from isophorone via one-step reaction, the dicyanoisophorone based fluorophore (**IS-NR-OH**) was synthesized according to the previous procedure [40]. Then, the control probe **IS-F** and probe **IS-NR-F** was easily prepared by the reaction of **IS-OH** or **IS-NR-OH** with tert-butyldimethylsilyl chloride in the presence of Et_3N at room temperature. The structures of the target **IS-F** and **IS-NR-F** and intermediates were characterized and confirmed by ^1H NMR, ^{13}C NMR, and HR-MS, as shown in **Figures S2-S16**.

3.2. Optical properties measurement

The absorption and emission spectra of fluorophores and probes (**IS-F** and **IS-NR-F**) were measured by the UV-vis and fluorescence spectra in PBS buffer solution (20 mM, pH=7.4, 50 % DMSO) at 37 °C. As shown in Fig.1, the fluorophore **IS-OH** and **IS-NR-OH** displayed a maximum absorption peak at 360 nm and 430 nm respectively, which were caused by the ICT process of the D-π-A structure. When excited, **IS-OH** (λ_{ex} = 440 nm) solution showed an optimal emission at 568 nm (Φ =0.092, using Fluorescein in 0.1 M NaOH as standard) and **IS-NR-OH** (λ_{ex} = 535 nm) showed an optimal emission at 665 nm (Φ = 0.083). This was because the

modification of isophorone with the strong electron-withdrawing malononitrile group could facilitate the ICT process, and also elongate the π-conjugation of the isophorone derivatives, which finally caused the emission colors turned from yellow-green to red. Meanwhile, the UV-Vis and fluorescence spectra response of control probe **IS-F** and **IS-NR-F** toward F^- were measured under the same condition. In absorbance spectra, the probe **IS-F** and **IS-NR-F** displayed a maximum absorption peak at 345 nm and 416 nm respectively. After the addition of F^- (8 ppm), the maximum absorption bands of two probe solutions red-shifted to 360 nm and 430 nm respectively. Accordingly, the addition of F^- could produce a significant color change, which can be used for naked-eye detection. In the fluorescent spectra, both probes **IS-F** (Φ = 0.0086) and **IS-NR-F** (Φ = 0.0057) showed weak emission due to the introduced tert-butyldimethylsilyl moiety occludes the ICT process. when F^- (8 ppm) was added, the emission intensity of probe **IS-F** and **IS-NR-F** solutions at 568 nm and 665 nm were dramatically increased respectively, and we also measured the excitation spectrum of the reaction solutions, the maximum excitation wavelengths of the **IS-F +** F^- and **IS-NR-F+** F^- were revealed at 446 nm and 538 nm respectively. The new absorption, excitation and emission peaks were quite similar to that of **IS-OH** and **IS-NR-OH**, which revealed that F^--induced desilylation reaction products ought to be their corresponding fluorophores, the Stokes shift of **IS-OH** and **IS-NR-OH** were found to be 122 nm and 127 nm respectively, which were calculated as the difference between the maximum excitation wavelengths and emission wavelengths. These initial results indicate that **IS-F** and **IS-NR-F** can be served as colorimetric and

fluorescent "turn-on" probe for rapid detection of F^-. Moreover, we found **IS-NR-F** showed obvious NIR emission enhancement around 665 nm for F^- and possesses a super large Stokes shift (127 nm), which is highly beneficial for biological application, as its low background interference, less photodamage, and deep penetration. In comparison, the bioimaging applications of probe **IS-F** may be limited due to its shorter emission wave. Therefore, in the following paper, we focused on the sensing properties of probe **IS-NR-F** for F^-.

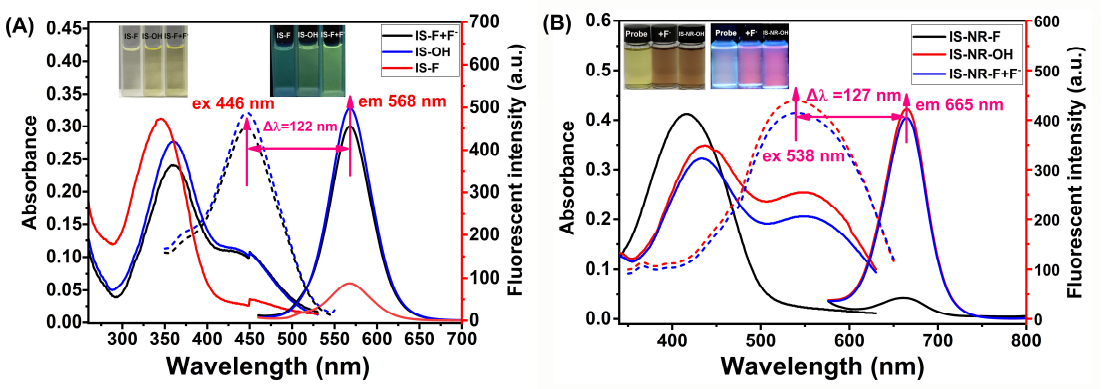

Fig. 1 (A) Absorption spectra and fluorescence spectra changes of probe **IS-F** (20 μM) upon addition of F^- (8 ppm) in PBS buffer solution (20 mM, pH=7.4, 50 % DMSO) at 37 °C. (B) Absorption spectra and fluorescence spectra changes of probe **IS-NR-F** (20 μM) upon addition of F^- (8 ppm) in PBS buffer solution (20 mM, pH=7.4, 50 % DMSO) at 37 °C. Insert: natural light color and emission color (under a 365 nm light).

In order to further study the optical properties of two probes, the photophysical properties of **IS-F, IS-O, IS-NR-F,** and **IS-NR-O** were performed density functional theory (DFT) calculations. The four molecular structures as well as the orbital electron cloud distribution, HOMO and LUMO energy were offered at the level of RB3LYP/6-311G (d) by the Gaussian 09 program. As exhibited in **Fig. 2**, all electron

clouds on HOMO and LUMO mainly focus on the whole π-conjugated chains, including C=O moiety and malononitrile group, and there is almost no electron cloud distribution on the side chain. The electrons on the aromatic ring attached to the negative ions of oxygen (O^-) in the LUMO orbital of **IS-O** and **IS-NR-O** were more dispersed than those of **IS-F** and **IS-NR-F** respectively. This could be interpreted as the significant ICT effect from the electron-donating phenoxy oxygen anion moiety to the carbonyl or dicyanoisophorone moiety. Nonetheless, we found the width of the electron cloud distribution of **IS-NR-F** and **IS-NR-O** were wider than that of **IS-F** and **IS-O**, which proved the malononitrile group elongates the π-conjugation of the isophorone. Moreover, the probe **IS-NR-F** has a smaller LUMO-HOMO energy gap (2.986 eV) than that of **IS-F** (3.691 eV), the result was in accord with the redshift of maximum absorption peak from 345 nm to 416 nm. Meanwhile, the negative ions **IS-NR-O** also has a smaller LUMO-HOMO energy gap (2.313 eV) than that of **IS-F** (2.595 eV), which in accord with the redshift of maximum absorption peak from 360 nm to 430 nm and emission peak from 568 nm to 665 nm.

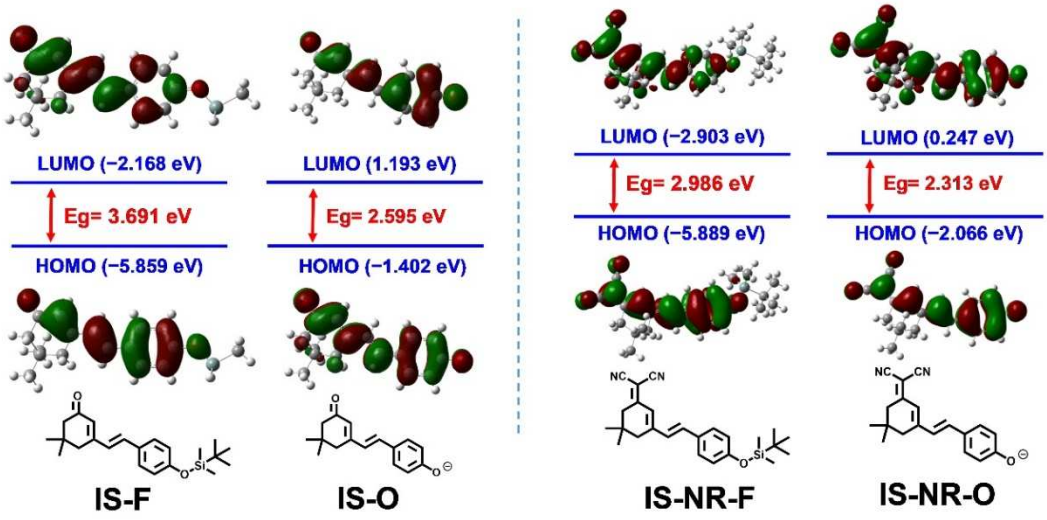

Fig. 2 The structural optimization of **IS-F, IS-O, IS-NR-F** and **IS-NR-O**

3.3. Sensing condition optimization

To explored the potential applications of **IS-NR-F**, the sensing conditions should be optimized, such as pH, temperature, solution system and time. Firstly, the intensity changes at 665 nm in different pH conditions of single **IS-NR-F** and toward F^- were investigated. As shown in **Fig. S17**, the results indicated that the fluorescent intensity of single **IS-NR-F** and toward F^- showed pH-dependence. The emission intensity of **IS-NR-F** solutions at 665 nm increased slowly in the range of 6.0-8.0 and increased drastically in the range of 8.0-11.0. When F^- added, the emission intensity at 665 nm increased drastically in the range of 6.0-8.0 and reached the peak value at pH=8.0 and then remained a plateau at 9-11. These results indicated that **IS-NR-F** would be suitable for detecting F^- in biological environments. Secondly, in view of the reaction-based **IS-NR-F,** we explored the influence of response time during the identification of F^-. As can be seen in **Fig. 3**, the fluorescence barely changed in the absence of F^-, while the fluorescent enhancement with varying degrees after a series of F^-(0.38, 1.9, 3.8, 5.7, 11.4 ppm) was added in DMSO/PBS buffer (1:1, v/v) (20 mM, pH=7.4) solution. When 11.4 ppm of F^- was added, the fluorescent intensity reached to a plateau within 25 min, which could be achieved with a *pseudo*-first-order rate constant (k´) for F^- calculated to be 0.136 min^{-1} (**Fig. S18**). To achieve the F^- detection in cells and take the pH range and temperature of biologically relevant into consideration, accordingly, the next experiment conditions were optimized to be carried out in a mixed solvent of 37 ºC and pH value of 7.4 for 25 minutes.

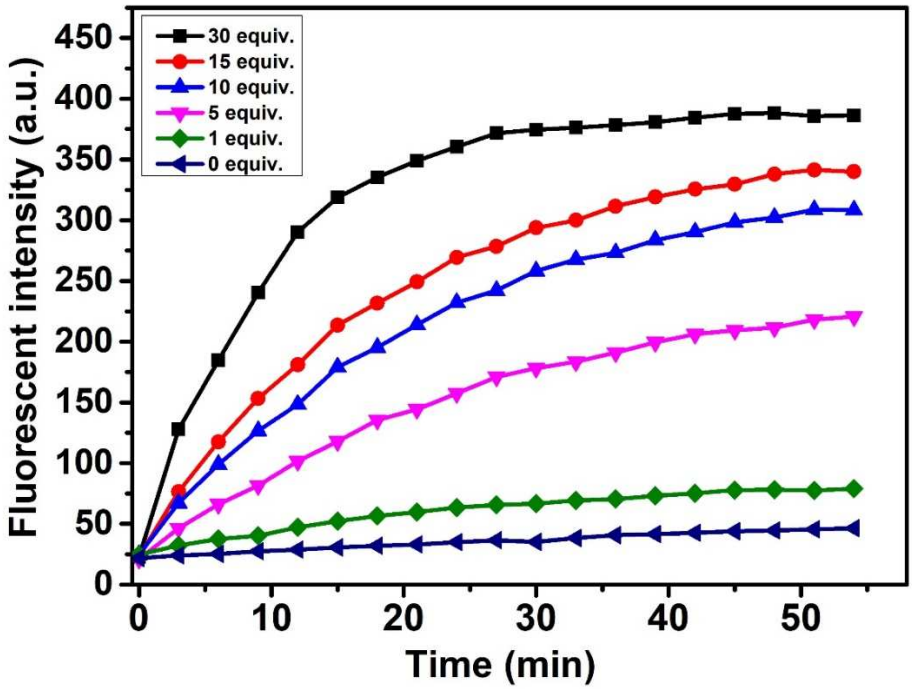

Fig. 3 The fluorescent intensity at 665 nm of **IS-NR-F** (20 μM) toward different F^- concentration (0.38, 1.9, 3.8, 5.7, 11.4 ppm) was continuously monitored at time intervals in DMSO/PBS buffer (1:1, v/v) (20 mM, pH=7.4) solution.

3.4. The sensing properties of probe IS-NR-F for F^-

The absorption spectra of **IS-NR-F** in the absence and presence of different F^- concentration was shown in **Fig. 4**. The **IS-NR-F** displayed a strong absorption peak at 416 nm in the absence of fluoride firstly. Interestingly, two new absorption peaks arose around 430 nm and 550 nm respectively with the addition of F^-, which were ascribed to the generation of **IS-NR-OH** and its deprotonation form (**IS-NR-O)** separately [71]. And the absorbance at 550 nm was enhanced gradually with the increasing concentrations of fluoride. What's more, a color change from yellow to brown was observed obviously in the presence of F^-, which meant that **IS-NR-F** could implement the "naked-eye" colorimetric recognition of F^-.

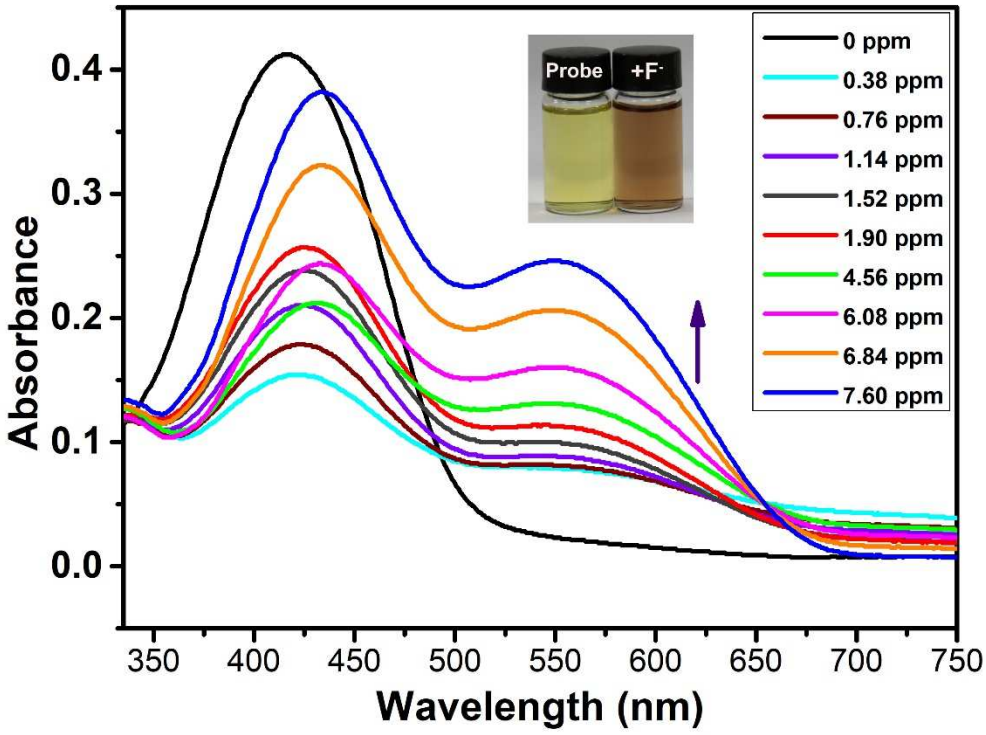

Fig. 4 UV-vis spectra changes of **IS-NR-F** (20 μM) with the addition of different concentrations of fluoride (0, 0.38, 0.76, 1.14, 1.52, 1.90, 4.56, 6.08, 6.84, 7.60 ppm) in PBS buffer solution (20 mM, pH=7.4, 50 % DMSO), inset: left: **IS-NR-F**, right: **IS-NR-F+F$^-$**

The fluorescent responses of probe **IS-NR-F** to F^- were recorded in **Fig. 5 (A)**. Initially, probe **IS-NR-F** (20 μM) itself displayed a slightly NIR fluorescence at 665 nm. It can be explained by the protection of the -OH with the tert-butyldimethylsilyl moiety, which hindered the intramolecular charge transfer (ICT) process. However, the NIR emissive fluorescence was augmented gradually with the titration of increasing F^- concentration. The NIR fluorescence at 665 nm was attributed to the resulting **IS-NR-O** after the reaction between **IS-NR-F** and F^-. As shown in **Fig. 5 (B)**, a wide detection range from 0.38-6.84 ppm with a good linearity relationship was achieved between the fluorescence of **IS-NR-F** and F^-, and the limit of detection

(LOD) was calculated to be 0.09 ppm based on the equation LOD=3 δ/k (δ was the standard deviation of the blank solution and k was the absolute value of the slope between fluorescence intensity and corresponding fluorine ion concentration) [72]. The LOD was much lower than the recommended fluoride level (1.5 ppm) in drinking water specified by WHO, which could give the credit to that the specific reaction induced by F^- improved the sensitivity. Moreover, the color changes of probe **IS-NR-F** toward F^- under natural light and handheld UV lamp (365 nm) was also performed, respectively. In natural light, the solution color gradually turned to brown in the presence of 0.38-7.6 ppm F^- and be more deepened with the increasing F^- concentration (**Fig. 5 (C)**). Similarly, the emission fluorescent color of **IS-NR-F** gradually turned to red with the increasing F^- concentration under hand-held UV lamp (365 nm) (**Fig. 5 (D)**), which meant that the color depth and fluorescent intensity would be enhanced gradually along with the increased concentration of F^-. Therefore, the probe **IS-NR-F** could achieve the naked eye and fluorescent colorimetric observation in the range of 0.38-7.6 ppm F^- in solution.

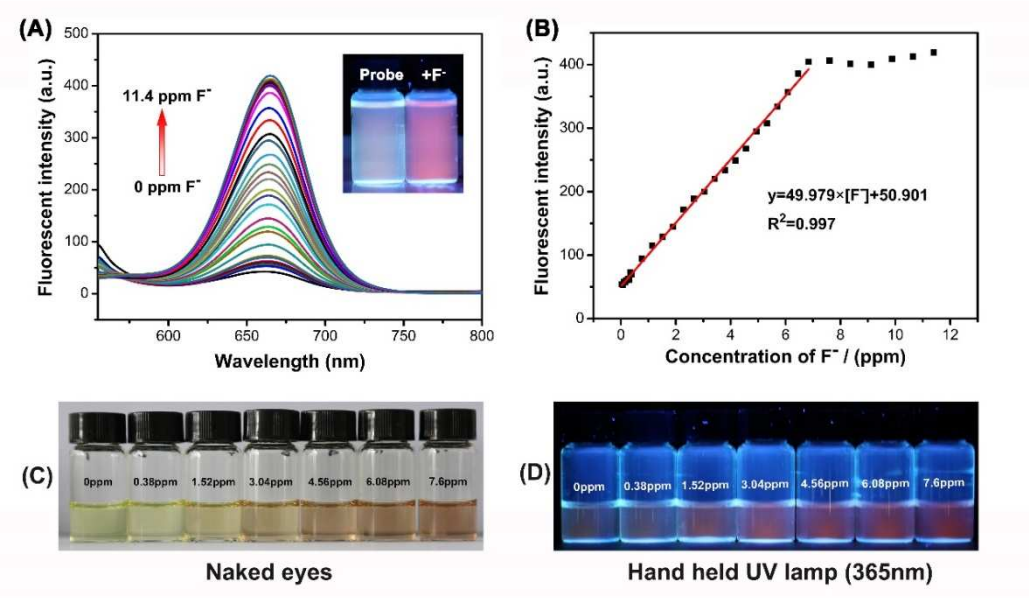

Fig. 5 (A) The changes of fluorescent emission intensity (at 665 nm) versus fluoride concentration (0-11.4 ppm), inset (Hand-held UV lamp at 365 nm): left: probe **IS-NR-F**, right: **IS-NR-F+F$^-$**; **(B)** The intensity linear relationship diagram of **IS-NR-F** (20 μM) toward different fluoride concentration (0-11.4 ppm) (at 665 nm); **(C)** and **(D)** The color changes and emission color changes of **IS-NR-F** toward various concentration of F$^-$ (0-7.6 ppm) were separately observed under naked eyes and hand held UV lamp (365 nm).

3.5. Selective experiment and colorimetric recognition

The selectivity of **IS-NR-F** was inquired by the fluorescent response of probe toward various relevant ions in organisms. When the system was in the presence of different 25 equiv. ions, including Cl^-, PO_4^{3-}, SO_3^{2-}, SO_4^{2-}, Ac^-, CO_3^{2-}, HCO_3^- , NO_2^-, NO_3^-, S^{2-}, Br^-, I^-, ClO^-, H_2O_2, Al^{3+}, Hg^{2+}, Mn^{2+}, K^+, Zn^{2+}, Ba^{2+}, Mg^{2+}, Cr^{3+}, Ca^{2+}, Pb^{2+}, Ag^+, Fe^{3+}, Ni^{2+}, Cu^{2+}, the responsive intensity of **IS-NR-F** toward them was quite weakly at 665 nm while a great fluorescence enhancement was acquired upon the addition of 25 equiv. F$^-$ **(Fig. 6 (A))**. The great contrast declared that **IS-NR-F**

exhibited an excellent selectivity to F^-, which could be ascribed to the strong affinity of F^- toward silicon. Apart from the excellent selectivity, **IS-NR-F** could be employed to the colorimetric recognition of F^- in the presence of different ions. As shown in **Fig. 6 (C)** and **(D)**, the specific cleavage reaction made the solution turn brown or produce a strong red fluorescence in the existence of F^- while there was no color change in the addition of other analytes. Hence, F^- could be easily recognized from other analytes whatever they were cations or anions or observed by naked eyes or hand-held UV lamp at 365 nm. In order to further estimate the resistant ability of **IS-NR-F** to other analytes during F^- detection, competitive experiments were carried out through adding F^- into the solution including different analytes directly **(Fig. 6 (B))**. It could be seen that the other analytes nearly performed slight interference on F^- detection. Therefore, probe **IS-NR-F** could be employed to recognize F^- specifically and colorimetry even in the existence of lots of common ions.

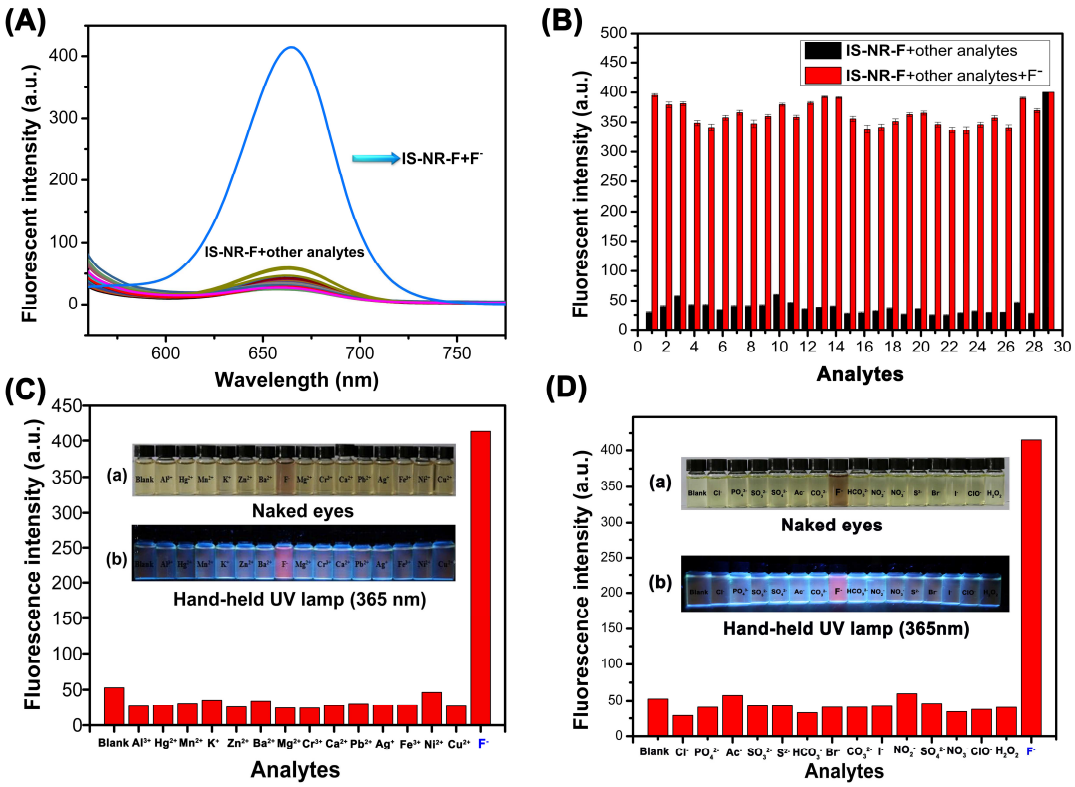

Fig. 6 **(A)** Fluorescence responses of probe **IS-NR-F** (20 μM) to various analytes (25 equiv.) in a mixture of DMSO and PBS buffer solution (pH=7.4, 20 mM), (1:1,v/v); **(B)** The competition experiment of **IS-NR-F** toward F^- in the presence of various analytes, including: 1:Cl^-, 2:PO_4^{3-}, 3:SO_3^{2-}, 4:SO_4^{2-}, 5:Ac^-, 6:CO_3^{2-}, 7:HCO_3^-, 8:NO_2^-, 9:NO_3^-, 10:S^{2-}, 11:Br^-, 12:I^-, 13:ClO^-, 14:H_2O_2, 15:Al^{3+}, 16:Hg^{2+}, 17:Mn^{2+}, 18:K^+, 19:Zn^{2+}, 20:Ba^{2+}, 21:Mg^{2+}, 22:Cr^{3+}, 23:Ca^{2+}, 24:Pb^{2+}, 25:Ag^+, 26:Fe^{3+}, 27:Ni^{2+}, 28:Cu^{2+}, 29:F^-; **(C)** and **(D)** were the colorimetric recognition of F^- in different cations and anions, respectively. All data were obtained after the reaction was conducted for 25 min at 37 ºC, λ_{ex}=535 nm, λ_{em}=665nm.

3.6. Detection mechanism studies

In order to verify our thoughts, the detection mechanism was investigated. According to the previous introduction, F^- could selectively cleave the Si-O bond. To

ascertain whether the turn-on NIR fluorescence response was attributed to the F^- induced Si-O bonds cleavage, therefore, ^1H NMR, ESI-MS and thin-layer chromatography (TLC) were carried out. The ^1H NMR spectrum was taken after purifying product from the reacting system. ^1H NMR spectrum of **IS-NR-F**, the purified reaction product, and the synthesized **IS-NR-OH** were shown in **Fig. 7**. When F^- was added, comparing the ^1H NMR spectra of **IS-NR-F** (**Fig. 7a**), fifteen protons of **IS-NR-F** corresponding to the protons of tert-butyldimethylsilyl group around 0.20 and 0.95 ppm disappeared (**Fig. 7c**), and a new proton peak emerged at 9.98 ppm, corresponding to the -OH. Especially, the purified product (**Fig. 7c**) displayed almost the same ^1H NMR spectrum with the synthesized **IS-NR-OH** (**Fig. 7b**). It indicated that the -OH emerged from the F^- induced Si-O bonds cleavage. And the detailed HR-MS analysis (**Fig. S19**) and TLC analysis (**Fig. S20**) further illustrated that the product of this reaction was **IS-NR-OH**.

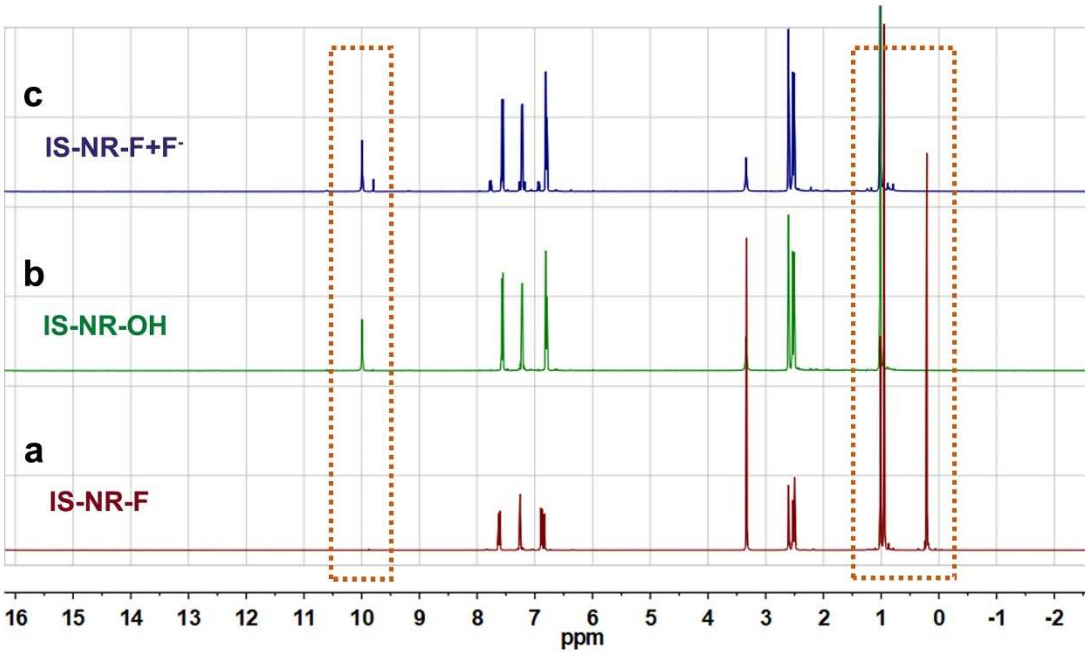

Fig. 7 Partial ^1H NMR spectra in DMSO-d_6: (a) only **IS-NR-F**, (b) the synthesized

IS-NR-OH, (c) the purified product after **IS-NR-F** reacted with F^-

3.7. F^- detection in aqueous sample and kinds of toothpaste

Given the widespread application of fluoride in our daily life, samples from tap water and the filtered Xiangjiang River in Hengyang were collected. The detective effects of probe **IS-NR-F** to F^- were exhibited in **Table 1**. The collected and treated water samples did not detect the presence of F^- in the case of that there was no additional F^- added. When samples were spiked with 0.38, 0.76, 1.52 ppm F^- respectively, all of the recoveries were in the range of 100-105 % after measured five times with the standard addition method. Besides, other ions in tap and river water didn't cause any obvious interference in the determination of F^- due to the strong affinity of F^- toward silicon. In the view of these results, probe **IS-NR-F** could be used to detect F^- in the actual aqueous sample successfully and selectively. Next, probe **IS-NR-F** was used to detect the content of F^- in some toothpaste samples. The tests of fluoride contents in toothpaste samples were listed in **Table 2** and the corresponding fluorescent spectra of these tests were shown in **Fig. S21**.

Table 1 F^- detection in actual water samples

Sample	Added F^- (ppm)	Detected (ppm)	Recovery (%)	RSD (%)
Tap water	0	0	-	-
	0.38	0.39	102.63	2.28
	0.76	0.78	102.63	2.17
	1.52	1.55	101.97	2.30
Xiangjiang river	0	0	-	-

	0.38	0.39	102.63	2.33
	0.76	0.79	103.94	2.07
	1.52	1.56	102.63	2.14

Table 2 The detection of F^- in commercially available toothpaste

Sample	Brand	F^- content (tested) mg/g	F^- content (marked) mg/g
1	Jiajieshi	0.11	0.11
2	Colgate	0.13	0.14
3	Oral-B	0.10	0.10
4	Bamboo salt	0.10	0.10
5	Zhonghua	0.12	0.14

3.8. Cells imaging and MTT assays

Taking the advantages of NIR emission and large Stokes shift into consideration, a standard cell viability protocols for investigating the biocompatibility of probe **IS-NR-F** toward HeLa cells were carried out first by MTT assay. As shown in **Fig. S22**, when the probe concentrations up to 50 μM, at least 90% of cells remained in good condition over 12 h. These results indicated that **IS-NR-F** had low cytotoxicity when the concentration was less than 50 μM, therefore, **IS-NR-F** was safe for the following bioimaging applications. For the next imaging experiment, 50 percent of HeLa cells were obtained after incubating an incubator for 12 hours, followed by the addition of **IS-NR-F** (20 μM contains 5 % DMSO) and incubated for 1 hour at 37 ºC.

And then the HeLa cells were washed with sterile PBS buffer solution for eliminating the interference of excess **IS-NR-F**. Finally, the fluorescent imaging was recorded after HeLa cells were treated with F^- for another 1 hour at 37 ºC. As shown in **Fig. 8**, there was a feeble fluorescence in the dark field when cells were merely treated with probe **IS-NR-F** (**Fig. 8 E, F, G**), illustrating that **IS-NR-F** was accessible to combine the F^- in cells and not responsive to the inside cell species. However, an apparent fluorescent enhancement was observed in the presence of F^-, and **IS-NR-F** performed an obvious red fluorescence that could decrease the background interference caused by the cell itself (**Fig. 8 I, J, K**). In addition, a reverse process of incubate the cell with fluoride first then add the probe were carried out to further confirmed the probe is able to detect the fluoride in cells. As shown in **Fig. S23**, only in the presence of F^-, no fluorescence signal can be observed in the dark field, when the cells were preincubated with F^- and then incubated with **IS-NR-F** for 30 min, an obvious enhanced red fluorescence can be clearly observed. Combining the characteristic of low cytotoxicity and successfully imaging assays together, it demonstrated that the probe **IS-NR-F** could be used for discerning F^- in cells.

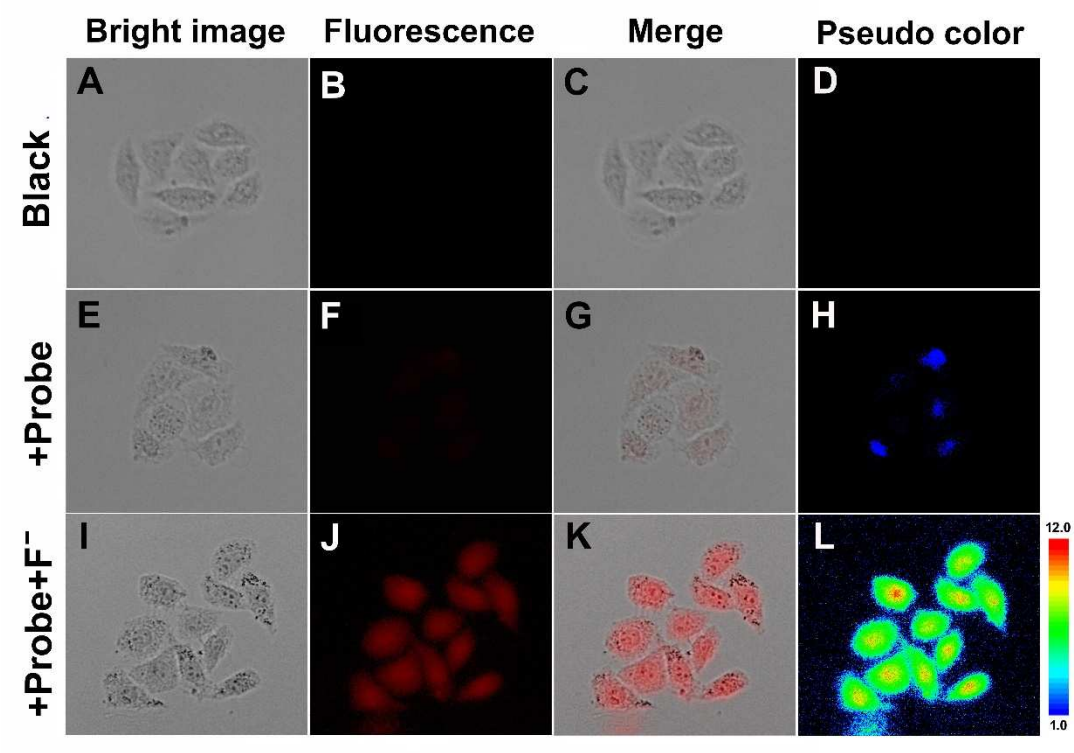

Fig. 8 Fluorescence images of untreated HeLa cells (A-D) and HeLa cells incubated with 20 μM of the **IS-NR-F** in the absence (E-H) and presence (I-L) of 3.8 ppm of fluoride ion. Corresponding bright field images (A, E, I), fluorescence field (B, F, J), merge images (C, G, K) and pseudo color (D, H, L) of HeLa cells were shown, respectively.

4. Conclusion

In summary, we have successfully designed and synthesized a dicyanoisophorone derivative-based colorimetric and near-infrared fluorescent probe **IS-NR-F** and an isophorone based control probe **IS-F** for the detection of fluorine ion by employing F^- selective cleavage of silicon-oxygen bonds. Fortunately, in the presence of F^-, the probe **IS-NR-F** exhibited a NIR fluorescence turn-on signaling at 665 nm with a remarkable Stokes shift (127 nm), which is more suitable for bioimaging application. The probe exhibited a wide detection range and very low

detection limit for fluorine ion, as well as selectively recognized fluorine ion in actual water samples including various ions present. Importantly, **IS-NR-F** has been successfully applied to detect fluorine ion in actual water samples and toothpaste extracted samples. Moreover, the probe toxicological experiments and near-infrared fluorescence imaging indicated that **IS-NR-F** was cell-permeable with low cytotoxicity and capable of real-time monitoring F^- in living cells. Taken together, our work provided a promising strategy for colorimetric and large Stokes shift near-infrared fluorescent probe for the anions monitoring in both real samples and living systems.

Conflicts of interest

There are no conflicts of interest to declare.

Acknowledgments

This work was supported by National Natural Science Foundation of China (No.11804146 and 11875161); Natural Science Foundation of Hunan Province (No.2016JJ5003); the Research Foundation of Education Bureau of Hunan Province (No.17B223); College Students' Innovation & Entrepreneurship Training Project of University of South China (No. 2018XJXZ332).

Reference:

[1] Dhillon A, Nair M, Kumar D. Anal. Methods. 2016; 8: 5338-5352.

[2] Beer P-D, Gale P-A. Angew. Chem. Int. Ed. 2001; 40: 486-516.

[3] Baker J-L, Sudarsan N, Weinberg Z, Roth A, Stockbridge R-B, Breaker R-R. Science 2012; 335: 233-235.

[4] Kirk K-L. In: Biochemistry of the Elemental Halogens and Inorganic Halides, Plenum Press, New York, 1991; pp 19-68.

[5] Kleerekoper M. Endocrin. Metab. Clin. 1998; 27: 441-452.

[6] Briançon D. Revue du rhumatisme (English ed.) 1997; 64: 78-81.

[7] Guidelines for drinking-water quality, in, World Health Organization, 2004; pp 375-377.

[8] Jiao Y, Zhu B-C, Chen J-H, Duan X-H. Theranostics 2015; 5: 173-187.

[9] Bassin E-B, Wypij D, Davis R-B, Mittleman M-A. Canc. Causes Contr. 2006; 17: 421-428.

[10] Bebeshko G-I, Karpov Y-A. Inorg. Mater. 2012; 48: 1335-1340.

[11] Breadmore M-C, Palmer A-S, Curran M, Macka M, Avdalovic N, Haddad P-R. Anal. Chem. 2002; 74: 2112-2118.

[12] Kumari N, Jha S, Bhattacharya S. J. Org. Chem. 2011; 76: 8215-8222.

[13] Kaur R, Sidhu J-S, Singh N, Kaur I, Kaur N. Sens. Actuator B-Chem. 2019; 293: 144-150.

[14] Tang, L-J, Tian, M-Y, Chen, H-B, Yan, X-M, Zhong, K-L, Bian, Y-J. Dyes. Pigm. 2018; 158: 482-489.

[15] Zhang, L, Liu, X-A, Gillis, K-D, Glass, T-E. Angew. Chem. Int. Ed. 2019; 58: 7611-7614.

[16] Xu, Ming, Kelley, S-P, Glass, T-E. Angew. Chem. Int. Ed. 2018; 57: 12741-12744.

[17] Yue, Y-K, Huo, F-J, Cheng, F-Q, Zhu, X-J, Mafireyi, T, Strongin, R-M, Yin, C-X. Chem. Soc. Rev. 2019; 48: 4155-4177.

[18] Yue, Y-K, Huo, F-J, Ning, P, Zhang, Y-B, Chao, J-B, Meng, X-M, Yin, C-X. J. Am. Chem. Soc. 2017; 139: 3181-3185.

[19] Yue, Y-K, Huo, F-J, Li, X-Q, Wen, Y, Yi, T, Salamanca, J, Escobedo, J-O, Strongin, R-M, Yin, C-X. Org. Lett. 2017; 19: 82-85.

[20] Xiong, K-M, Huo, F-J, Chao, J-B, Zhang, Y-B, Yin, C-X. Anal. Chem. 2019; 91: 1472-1478.

[21] Yue, Y-K, Huo, F-J, Yin, C-X. Anal. Chem. 2019; 91: 2255-2259.

[22] Wu Y-L, Wang J, Zeng F, Huang S-L, Huang J, Xie H-T, Yu C-M, Wu S-Z. ACS Appl. Mater. Inter. 2016; 8: 1511-1519.

[23] Hu Q-H, Yu C-M, Xia X-T, Zeng F, Wu S-Z. Biosens. Bioelectron. 2016; 81: 341-348.

[24] Gao W-D, Li H, Zhang Y-P, Pu S-Z. Tetrahedron 2019; 75: 2538-2546.

[25] Liu B, Tan Y-H, Hu Q-H, Wang Y-Y, Mao Y, Tao P, Wang H-Q. Sens. Actuator B-Chem. 2019; 296: 126675.

[26] Ghosh S, Bhamore J-R, Malek N-I, Murthy Z, Kailasa S-K. Spectroc. Acta Pt. A-Molec. Biomolec. Spectr. 2019; 215: 209-217.

[27] Bhamore J-R, Jha S, Park T-J, Kailasa S-K. Sens. Actuator B-Chem. 2018; 277: 47-54.

[28] Zhao Y-P, Ma Y-Y, Lin W-Y. Sensor Actuat. B-Chem. 2019; 288: 519-526.

[29] Xie X-L, Li M-M, Tang F-Y, Li Y, Zhang L-L, Jiao X-J, Wang X, Tang B. Anal.

Chem. 2017; 89: 3015-3020.

[30] Sedgwick A-C, Wu L-L, Han H-H, Bull S-D, He X-P, James T-D, Sessler J-L, Tang B-Z, Tian H, Yoon J. Chem. Soc. Rev. 2018; 47: 8842-8880.

[31] Bains D, Singh G, Singh N. Tetrahedron Lett. 2019; 60: 1457-1462.

[32] Tang A-L, Yin Y, Chen Z, Fan C-B, Liu G, Pu S-Z. Tetrahedron 2019; 74: 130489.

[33] Erdemir S, Yuksekogul M, Karakurt S, Kocyigit O. Sensor Actuat. B-Chem. 2017; 241: 230-238.

[34] Xie X-X, Yin C-X, Yue Y-K, Huo F-J. Sensor Actuat. B-Chem. 2018; 267: 76-82.

[35] Cheng D, Peng J-J, Lv Y, Su D-D, Liu D-J, Chen M, Yuan L, Zhang X-B. J. Am. Chem. Soc. 2019; 141: 6352-6361.

[36] Wu D, Chen L-Y, Lee W, Ko G, Yin J, Yoon J. Coordin. Chem. Rev. 2018; 354: 74-97.

[37] Liu X-J, Tian H-H, Yang L, Su Y-A, Guo M, Song X-Z. Sensor Actuat. B-Chem. 2018; 255: 1160-1165.

[38] Qi F-P, Liu X-J, Yang L, Yang L, Chen W-Q, Song X-Z. Tetrahedron 2016; 72: 6909-6913.

[39] Zhu J-Y, Zhou L-F, Y Li-K, Chen S-B, Yan J-W, Zhang L. Anal. Chim. Acta 2017; 961: 112-118.

[40] Wang K, Leng T-H, Liu Y-J, Wang C-Y, Shi P, Shen Y-J, Zhu W-H. Sensor Actuat. B-Chem. 2017; 248: 338-345.

[41] Du M, Huo B-L, Liu J-M, Li M-W, Fang L-Q, Yang Y-X. Anal. Chim. Acta 2018;

1030: 172-182.

[42] Zou B, Liu H, Mack J, Wang S-S, Tian J-W, Lu H, Li Z-F, Shen Z. RSC Adv. 2014; 4: 53864-53869.

[43] Liu J-W, Yin Z. Talanta 2019; 196: 352-356.

[44] Han J-L, Zhang J, Gao M-Q, Hao H-P, Xu X-W. Dyes. Pigm. 2018; 162: 412-439.

[45] Yuan X, Xu X-J, Zhao C-X, Zhang F, Lu Y-X, Shen Y-J, Wang C-Y. Sensor Actuat. B-Chem. 2017; 253: 1096-1105.

[46] Wu J-F, Lai G-Q, Li Z-F, Lu Y-X, Leng T-H, Shen Y-J, Wang C-Y. Dyes. Pigm. 2016; 124: 268-276.

[47] Gonçalves A-C, Sato N-C, Santos H-M, Capelo J-L, Lodeiro C, Santos A-A. Dyes. Pigm. 2016; 135: 177-183.

[48] Malkondu S, Altinkaya N, Erdemir S, Kocak A. Sensor Actuat. B-Chem. 2018; 276: 296-303.

[49] Kumar G-G-V, Kesavan M-P, Sivaraman G, Rajesh J. Sensor Actuat. B-Chem. 2018; 255: 3194-3206.

[50] Anand T, Sivaraman G, Iniya M, Siva A, Chellappa D. Anal. Chim. Acta 2015; 876: 1-8.

[51] Zheng X-J, Zhu W-C, Liu D, Ai H, Huang Y, Lu Z-Y. ACS Appl. Mater. Inter. 2014; 6: 7996-8000.

[52] Qi F-P, Zhang F, Mo L-N, Ren X-J, Wang Y-G, Li X, Liu X-J, Zhang Y, Yang Z-G, Song X-Z. Spectroc. Acta Pt. A-Molec. Biomolec. Spectr. 2019; 219: 547-551.

[53] Zhou Y, Zhang J-F, Yoon J. Chem. Rev. 2014; 114: 5511-5571.

[54] Li D-M, Zhong Z-M, Zheng G-X, Tian Z-Z. Spectroc. Acta Pt. A-Molec. Biomolec. Spectr. 2017; 185: 173-178.

[55] Ashokkumar P, Weißhoff H, Kraus W, Rurack K. Angew. Chem. Int. Ed. 2014; 53: 2225-2229.

[56] Chen X-X, Leng T-H, Wang C-Y, Shen Y-J, Zhu W-H. Dyes. Pigm. 2017; 141: 299-305.

[57] Swamy K, Lee Y-J, Lee H-N, Chun J, Kim Y, Kim S-J, Yoon J. J. Org. Chem. 2006; 71: 8626-8628.

[58] Zhao H-Y, Leamer L-A, Gabbaï F-P. Dalton. Trans. 2013; 42: 8164-8178.

[59] Wade C-R, Broomsgrove A-E, Aldridge S, Gabbai F-P, Chem. Rev. 2010; 110: 3958-3984.

[60] Yuan M-S, Wang Q, Wang W-J, Wang D-E, Wang J-R, Wang J-Y. Analyst 2014; 139: 1541-1549.

[61] Kim T-H, Swager T-M. Angew. Chem. Int. Ed. 2003; 42: 4803-4806.

[62] Zhang S, Sun M-T, Yan Y-H, Yu H, Yu T, Jiang H, Zhang K, Wang S-H. Anal. Bioanal. Chem. 2017; 409: 2075-2081.

[63] Zhou Y, Liu M-M, Li J-Y, Ye M-A, Yao C. Dyes. Pigm. 2018; 158: 277-284.

[64] Ke B-W, Chen W-X, Ni N-T, Cheng Y-F, Dai C-F, Dinh H, Wang B-H. Chem. Commun. 2013; 49: 2494-2496.

[65] Shi X-M, Fan W-L, Fan C-H, Lu Z-L, Bo Q-B, Zhuo W, Black C-A, Wang F-F, Wang Y-Q. Dyes. Pigm. 2017; 140: 109-115.

[66] Zhu B-C, Yuan F, Li R-X, Li Y-M, Wei Q, Ma Z-M, Du B, Zhang X-L. Chem. Commun. 2011; 47: 7098-7100.

[67] Wei G-H, Yin J-X, Ma X, Yu S-Y, Wei D-B, Du Y-G. Anal. Chim. Acta 2011; 703: 219-225.

[68] Dhanunjayarao K, Mukundam V, Venkatasubbaiah K. Sens. Actuator B-Chem. 2016; 232: 175-180.

[69] Sokkalingam P, Lee C-H. J. Org. Chem. 2011; 76: 3820-3828.

[70] Zhang J-F, Lim C-S, Bhuniya S, Cho B-R, Kim J-S. Org. Lett. 2011; 13: 1190-1193.

[71] Wang K, Zhao C-X, Leng T-H, Wang C-Y, Lu Y-X, Shen Y-J, Zhu W-H. Dyes. Pigm. 2018; 151: 194-201.

[72] Zheng S-L, Wang H-H, Hu Q-H, Wang Y-Y, Hu J-K, Zhou F-F, Liu P-Y. Sensor Actuat. B-Chem. 2017; 253: 766-772.

Highlights

1) A new dicyanoisophorone derived near-infrared emissive fluorescent probe (**IS-NR-F**) was synthesized with a large Stokes shift (127 nm).

2) The probe performed an excellent selectivity for F^- by naked eyes.

3) The probe exhibited a wide detection range with a good linear relationship for F^-.

4) The probe was applied to detect F^- in toothpaste samples and imaging in living cells.

Declaration of interests

☒ The authors declare that they have no known competing financial interests or personal relationships that could have appeared to influence the work reported in this paper.

☐The authors declare the following financial interests/personal relationships which may be considered as potential competing interests: